Two-photon excitation spectroscopy of Cr^{3+}:K_2NaScF_6 elpasolite: I. Experimental aspects

2001 J. Phys.: Condens. Matter 13 2363

(http://iopscience.iop.org/0953-8984/13/10/327)

INSTITUTE OF PHYSICS PUBLISHING JOURNAL OF PHYSICS: CONDENSED MATTER

J. Phys.: Condens. Matter **13** (2001) 2363–2375 www.iop.org/Journals/cm PII: S0953-8984(01)16926-2

Two-photon excitation spectroscopy of Cr^{3+}:K_2NaScF_6 elpasolite: I. Experimental aspects

G R Wein[1], D S Hamilton, U Sliwczuk[2], A G Rinzler[3] and R H Bartram

Department of Physics and Institute of Materials Science, University of Connecticut, Storrs, CT 06269, USA

Received 7 September 2000, in final form 8 January 2001

Abstract

Two-photon excitation experiments were performed to improve understanding of electron–lattice coupling and its effects on intra-$3d^3$ transitions. Cr^{3+} occupies a scandium octahedral site in K_2NaScF_6. The transitions studied were ${}^4A_{2g} \rightarrow {}^4T_{2g}$ and ${}^4A_{2g} \rightarrow {}^4T_{1ag}$. Complete spectra were recorded at a temperature of 10 K with the polarization vector $\hat{\boldsymbol{\eta}}$ parallel to the $\langle 100 \rangle$ or $\langle 110 \rangle$ crystallographic direction. The two bands exhibit different polarization anisotropies and phonon couplings. The electric-dipole-forbidden ${}^4A_{2g} \rightarrow {}^4T_{2g}$ band appears to be built on an e_g-mode false origin and contains Fano antiresonances. This broad transition band lacks a zero-phonon line or any other sharp structure. The ${}^4A_{2g} \rightarrow {}^4T_{1ag}$ transition zero-phonon line is evident and shows a 163 cm^{-1} low-temperature phase-transition-induced splitting. It also contains an extended progression of 35 phonon peaks corresponding to a lattice mode with phonon energy 106 cm^{-1}, and a second progression with phonon energy 310 cm^{-1}. The very asymmetric phonon side band displays a polarization anisotropy that differs from that of the zero-phonon line. To facilitate analysis of the data, measurements of low-temperature ${}^4T_{2g} \rightarrow {}^4A_{2g}$ emission spectra with one-photon excitation are also reported and interpreted in the present paper.

1. Introduction

Two-photon-excitation (TPE) spectroscopy of Cr^{3+}:K_2NaScF_6 was performed to provide a better understanding of electron–lattice coupling and its effects on intra-$3d^3$ transitions. The present paper describes the experiment and its results. Theoretical approaches used in the analysis of the data are developed in the following paper [1], henceforth designated II.

There have been several successes recently in the development of wavelength-tunable near-infra-red and infra-red solid-state lasers: Ti:sapphire [2], Co:MgF_2 [3], Cr:forsterite [4],

[1] Present address: St George's School, PO Box 1910, Newport, RI 02840, USA.

[2] Present address: Regierungspräsidium Kassel, Staatliches Umweltampt, Otto-Hahn-Strasse 5, D-34123 Kassel, Germany.

[3] Present address: Department of Physics, University of Florida, Gainesville, FL 32611-8440, USA.

0953-8984/01/102363+13$30.00

alexandrite [5], and the chromium-doped colquiriites, LiCAF [6], LiSAF [7], and LiSGAF [8]. In all of these cases the transition-metal-ion dopants provide the lasing action.

Trivalent cation dopants in elpasolites substitute for octahedrally coordinated metal ions. This local environment has been exploited recently in correlation crystal field calculations [9], energy transfer dynamics [10, 11] and other two-photon experiments [12]. Elpasolites have also been used as hosts for Ce^{3+}, resulting in excellent scintillator materials [13].

The present material, Cr^{3+}:K_2NaScF_6, was developed originally as a potential tunable laser material. The relevant processes involved in vibronic lasers are explained in McCumber's work on phonon-terminated four-level lasers [14, 15]. One limitation of this model is the exclusion of electronic states not involved in the lasing, and any effects these states introduce. In the material investigated here, Cr^{3+}:K_2NaScF_6, the other excited states of the Cr^{3+} ion give rise to a broad excited-state-absorption (ESA) band. The ESA severely degrades laser performance by limiting the possible tuning range [16]; it was suggested that the inclusion of more than one active phonon mode may provide an explanation. In an elaboration of this concept, Caird *et al* [17] suggested that equal but oppositely directed coupling to degenerate e-modes could account for an observed broad ESA band in $Na_3Ga_2Li_3F_{12}$:Cr^{3+}. An objective of the present experiment is to determine whether or not two excited states of Cr^{3+}:K_2NaScF_6, $^4T_{2g}$ and $^4T_{1ag}$, are coupled to the same modes with the same strength. Evidence will be presented here and in the subsequent theoretical paper that a single configuration coordinate does not adequately represent the phonon coupling in the present system.

Apart from their potential as laser materials, chromium-doped halide elpasolites provide model systems for investigating crystal-field and vibronic-coupling effects since the elpasolite structure can accommodate a substitutional trivalent cation impurity in a site of rigorous octahedral symmetry without charge compensation. The electronic states of interest are the $^4A_{2g}$, $^4T_{2g}$ and $^4T_{1ag}$ states, all derived from the free-ion $3d^3$ ground configuration of Cr^{3+} as indicated by the Tanabe–Sugano diagram [18] shown in figure 1, and therefore all of the same parity. Unfortunately, one-photon electric-dipole transitions between states of the same parity are forbidden by the inversion symmetry of the substitutional site. Two-photon electric-dipole transitions are parity allowed, however, and the most relevant advantage of two-photon excitation spectroscopy is its ability to record vibronic spectra unobscured by false origins or other odd-symmetry modes apparent in parity-forbidden one-photon transitions. This advantage, which enables measurement of the coupling of each transition to each even mode of the CrF_6^{3-} octahedron, a_{1g}, e_g and t_{2g}, was exploited in a previous investigation of a closely related material, Cr^{3+}:K_2LiGaF_6 [19]. It will become apparent that some results of the present investigation are significantly different by virtue of a low-temperature phase transition in Cr^{3+}:K_2NaScF_6, revealed by Raman spectroscopy [20], which diminishes its efficacy as a model system but introduces novel features of TPE spectra.

The material studied here, generously provided by GTE, has been included in several other investigations as well. Thermal quenching of luminescence, investigated by photoluminescence spectroscopy at both ambient pressure [21] and high pressure [22], gave insights into crystal-field effects on non-radiative transition rates. Related theoretical investigations were conducted of lattice dynamics [23], optical properties [24] and thermal quenching of luminescence [25, 26].

Excitation spectra associated with two-photon $^4A_{2g} \rightarrow {}^4T_{1ag}$ and $^4A_{2g} \rightarrow {}^4T_{2g}$ transitions were monitored by one-photon $^4T_{2g} \rightarrow {}^4A_{2g}$ emission, as indicated in figure 1. Second-order time-dependent perturbation theory can be used within the electric-dipole approximation for a single laser beam of frequency ω to derive an expression for the two-photon transition probability that exhibits quadratic dependence on the incident laser intensity, I_0. The quadratic dependence of the emitted intensity I on the incident intensity I_0 was

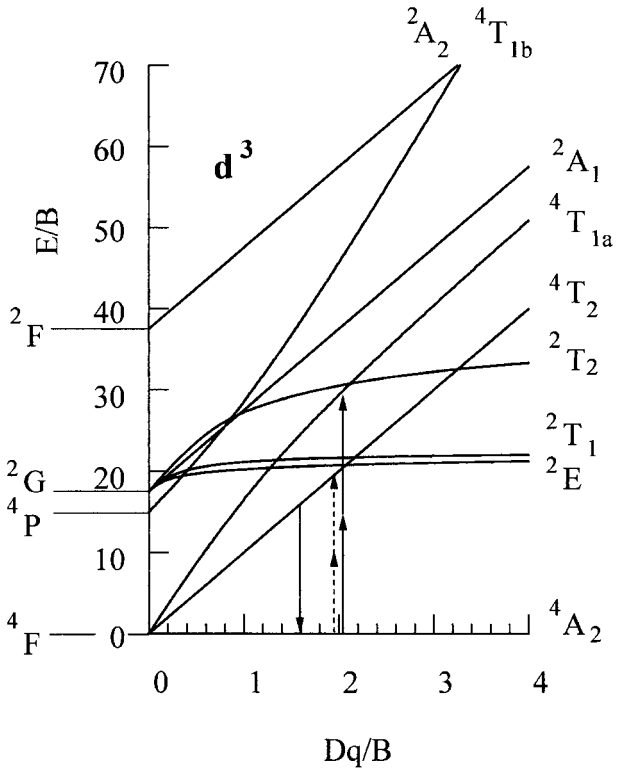

Figure 1. Tanabe–Sugano diagram for a d^3 ion in octahedral coordination, with positions of the two-photon excitation and emission transitions in Cr^{3+}:K_2NaScF_6 indicated.

verified experimentally, thus confirming that excitation spectra were in fact two-photon spectra. Therefore, the signal was always normalized to I_0^2 during the experiment. Polarization anisotropy in two-photon absorption (TPA), which was considered for all 32 crystallographic point groups by Bader and Gold [27], was investigated as a function of wavelength for each of the TPE spectra recorded. The one-photon $^4T_{2g} \rightarrow {}^4A_{2g}$ emission spectrum was recorded in a separate experiment.

2. Experimental aspects

Parity-allowed TPA transitions have cross sections that are typically in the 10^{-51} to 10^{-54} cm^4 s range [28]. High peak powers were therefore needed if a significant amount of Cr^{3+} emission was to be generated. There was a one gigawatt per square centimetre upper limit for the excitation intensity because of the crystal's damage threshold. The design of the experiment was then dictated by keeping the power below the damage threshold but large enough to produce a signal-to-noise ratio in excess of 2:1.

The complete apparatus, shown in figure 2, was based on a Nd:YAG-pumped tunable dye laser passing through a hydrogen gas filled Raman shifter. The first order shift was used to investigate the $^4A_{2g} \rightarrow {}^4T_{1ag}$ band while the second-order shift provided the excitation for the $^4A_{2g} \rightarrow {}^4T_{2g}$ band. The photon energy of the output beam was shifted by a constant 4155 cm^{-1} in the first order and twice this amount in the second order.

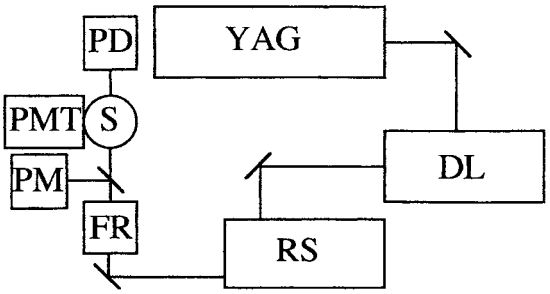

Figure 2. Two-photon excitation optical design showing the DCR-11 YAG laser (YAG) pumping the three-stage dye laser (DL) followed by the Quanta Ray model RS-1 Raman shifter (RS). The sample (S) is held in a closed-cycle helium cryostat. The emission is collected by the photomultiplier (PMT) while the laser energy is recorded by a germanium photodiode (PD). The Fresnel rhombs act as an achromatic half-wave plate to rotate the polarization vector. Kinematic mounts move mirrors into the beam to monitor the wavelength and laser power with a Scientech power meter (PM).

The second harmonic of a Quanta-Ray DCR-11 YAG laser, with a nominal pulse duration of 10 ns, was the pump source for a three-stage wavelength tunable dye laser built specifically for this experiment. The dye laser tuning range required to cover both transitions was 595 to 700 nm. The dyes used were Rhodamine B, Rhodamine 640, DCM and LD688, all purchased from Exciton Inc. Concentration and solvent shifting of the tuning ranges were used to assure the peak dye laser power stayed at least a factor of two over the Raman shifter threshold.

The Quanta Ray RS-1 Raman shifter converted this tuning range to 790 to 987 nm and 1178 to 1670 nm. The linewidth of the dye laser was calculated, based on the Littrow design, to be approximately 0.15 cm^{-1}. This linewidth was maintained as the beam passed through the Raman shifter. The RS-1 used a Pellin-Broca prism to separate the different orders. The inherently dispersive nature of this element caused movement of the beam as the dye laser wavelength was scanned. To compensate for this a stepping motor was attached to the micrometer drive of the prism table and the computer kept the infrared beam stationary.

Achromatic polarization rotation was achieved by using a matched pair of Fresnel rhombs. Through the careful alignment of the retroreflected spots, as viewed with an IR scope, the rhombs could be rotated without deflecting the laser beam. This was essential to eliminate any effects caused by beam wander in the crystal or on the reference detector.

The crystal was held by an oxygen-free-copper spring mount at a temperature of 10 K in an APD displex model DE202. The crystal was x-ray oriented and held with the $\langle 001 \rangle$ direction parallel to the optic axis. Emission was collected along the $\langle 100 \rangle$ direction. Poor mechanical properties of the crystal prevented the use of a thermally conducting epoxy so Wakefield 120 paste was utilized.

The crystal can only radiatively emit from the $^4T_{2g}$ state because absorption into the $^4T_{1ag}$ and other higher states decays non-radiatively into the lower $^4T_{2g}$ state. Therefore the simultaneous absorption of two photons into any state was detected by collecting the $^4T_{2g} \rightarrow {}^4A_{2g}$ emission. The Hamamatsu 928R photomultiplier tube used to collect emission was therefore fitted with a stack of broadband filters to allow as much signal as possible without passing scattered excitation or stray pump light. The filter stack passed approximately 40 nm, from 680 to 720 nm.

The detection electronics consisted of a computer-controlled Stanford Research System dual-channel gated photon counter, model SR400, and two gated integrators, model SR250. The photon counter, triggered by the DCR-11 Q-switch synchronization pulse, counted current

pulses corresponding to emission photons in two 600 μs windows. The windows and the delays were chosen because the measured emission lifetime was 580 μs [21]. The first time window, starting 10 μs after the laser pulse to avoid stray light and RF pickup in the photomultiplier preamplifier, was still within the first lifetime. The second window was delayed by 4 ms and was used for the background measurement because the small emission signal had decreased into the background dark current by this delay. The two-photon excitation signal was then the difference of the photon counts in the two windows calculated after each laser pulse.

Two gated integrators were used to measure the laser intensity and reference output of a Germanium Power Devices GM-4 photodiode, sensitive in the infrared from 0.8 to 1.8 μm. After each laser pulse the laser intensity was calculated as the difference of the two gated integrator outputs.

Two hundred measurements were appropriately normalized, and then averaged for each data point. Normalization consisted of dividing the background-corrected emission signal by the square of the background-corrected laser intensity on a shot-by-shot basis.

To ensure that the dye-laser wavelength was scanning correctly and that the damage threshold was not being approached, data were taken in 10–15 nm increments. The resulting spectra were overlapped and spliced together, by matching magnitude and slope, to form a complete two-photon excitation spectrum of each band for each polarization orientation. This 'cut and paste' technique avoided the anomalies introduced into nonlinear optical spectra by mode and pulse width changes near the end of dye tuning curves [29, 30].

In a separate experiment, the emission spectrum of Cr^{3+}:K_2NaScF_6 was recorded with the sample maintained at 2.1 K. One-photon excitation was provided by the 457.9 nm line of a Spectra Physics 2025-5 argon-ion laser. Dispersion of the sample luminescence was performed by a Spex 1404, 0.85 m double monochromator equipped with Bausch and Lomb 110×110 mm^2, 1800 grooves mm^{-1} holographic gratings. The spectrometer entrance and exit slit widths were each set at 50 mm with the two internal slits both at 600 mm. Luminescence was detected by an RCA 31034C GaAs photomultiplier tube. Current from the photomultiplier tube was converted to a proportional voltage by a Keithley 610C electrometer and recorded by a strip chart recorder.

3. Experimental results

3.1. $^4T_{2g} \rightarrow {}^4A_{2g}$ *emission spectrum*

The full $^4T_{2g} \rightarrow {}^4A_{2g}$ fluorescence spectrum is shown in figure 3. As in other low-field complexes, this is the only radiative emission of the Cr^{3+} ion. Wavelengths and energies of the numbered peaks and their energies relative to the zero-phonon line are listed in table 1. The observed structure has been interpreted in terms of the normal modes of the CrF_6^{3-} octahedral complex. Peak assignments listed in table 1 were made by comparison with the analogous Cr^{3+}-doped elpasolite Cr^{3+}:K_2NaGaF_6 [31, 32], with a very similar fluorescence spectrum, and confirmed by high-pressure photoluminescence [22] and Raman spectroscopy [20]. Although a distinct t_{2g}-mode peak was not observed, its existence was inferred from the observation of the t_{2g} line in the gallium elpasolite. From its position in that crystal, a peak corresponding to the t_{2g} mode was assumed to be the cause of the shoulder on the low-energy side of the scandium crystal t_{2u} line, and its position was crudely estimated. The t_{2g} mode has been observed separately in pressure dependent $^2E_g \rightarrow {}^4A_{2g}$ emission [22] and Raman spectroscopy [20]. Interpretation of the data in those works yields a t_{2g} vibrational energy of 232 cm^{-1}, in close agreement with the 228 cm^{-1} estimated from the present low-temperature fluorescence spectrum. The emission spectra of the chromium-doped elpasolite Cr^{3+}:K_2NaGaF_6 was also

recorded at the temperature of 2.1 K. Positions of the $^4T_{2g} \rightarrow {}^4A_{2g}$ resolved structure in that spectrum agree, to within the listed experimental uncertainty, with the line positions reported by Ferguson *et al* [31].

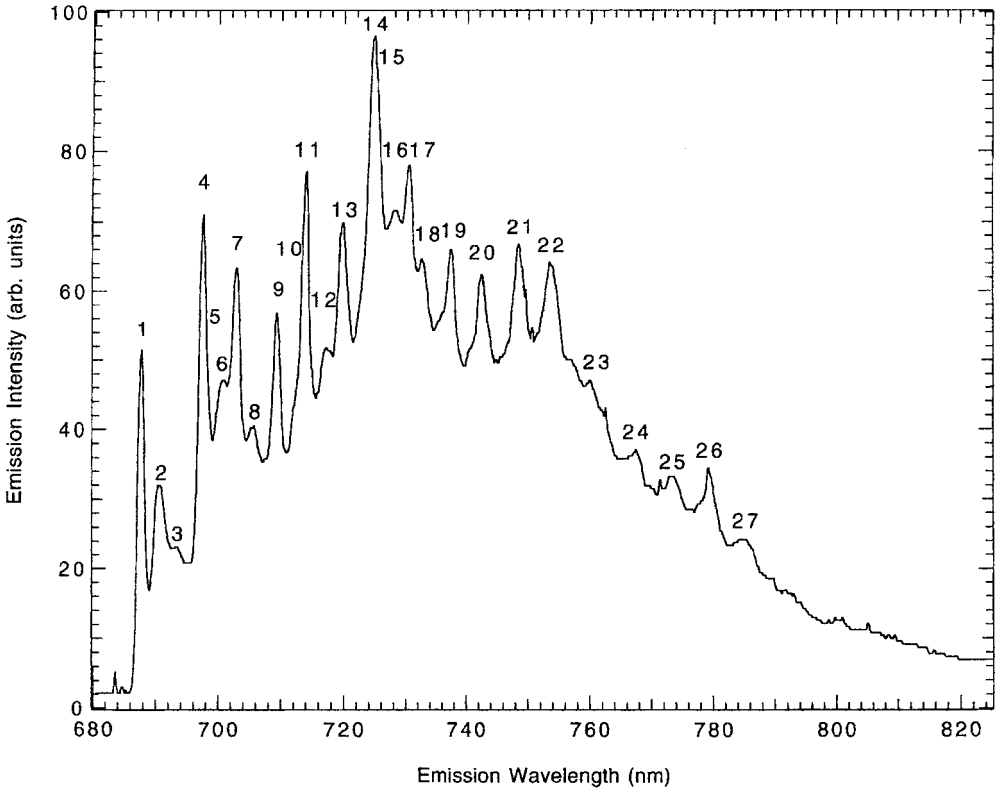

Figure 3. Emission spectrum of Cr^{3+}:K_2NaScF_6 at 2.1 K. The 27 phonon peak assignments are given in table 1.

The scandium elpasolite undergoes a phase transition to lower than octahedral symmetry below room temperature, as evidenced by Raman scattering [20]. This phase transition is also manifest in a split zero-phonon line and split phonon replicas in the high-pressure, low-temperature photoluminescence spectrum recorded at 6.3 GPa and 149 K [22]. The observed splitting is a consequence of the removal of orbital degeneracy in the $^4T_{2g}$ excited state, since the $^4A_{2g}$ ground state is orbitally non-degenerate. The two components of the zero-phonon line, which are separated by approximately 20 cm^{-1}, are of nearly comparable intensity at 149 K, since the higher-energy component of the excited state is thermally populated from the lower-energy component following optical excitation. However, at 2.1 K with the same splitting, the population of the higher-energy component would be diminished by six orders of magnitude relative to that of the lower-energy component; accordingly, no split zero-phonon line or split phonon replicas should be observable in figure 3. The relatively large width and asymmetry of the zero-phonon line may be an indirect manifestation of the phase transition.

Table 1. Experimental positions of the 27 numbered peaks of figure 3. The energy of each peak relative to that of the zero-phonon line and its assigned normal-mode designation are also listed.

Line number	Wavelength (nm)	Energy (cm^{-1})	Vibrational energy (cm^{-1})	Assignment
1	687.3	14 549 ± 3	—	zero-phonon
2	690.3	14 486 ± 4	63	lattice
3	693.1	14 428 ± 5	121	lattice
4	698.1	14 342 ± 3	207	t_{2u}
5	698.3	14 321 ± 15	228	t_{2g}
6	700.3	14 279 ± 4	270	$t_{2u} + 63$
7	702.6	14 233 ± 3	316	t_{1u}
8	705.4	14 176 ± 4	373	$t_{1u} + 63$
9	709.2	14 100 ± 3	449	e_g
10	712.1	14 043 ± 8	506	$e_g + 63$
11	713.9	14 007 ± 3	542	a_{1g}
12	717.1	13 946 ± 4	603	$a_{1g} + 63$
13	719.8	13 893 ± 4	656	$t_{2u} + e_g$
14	724.5	13 802 ± 5	747	$t_{2u} + a_{1g}$
15	725.7	13 780 ± 6	769	$t_{1u} + e_g$
16	727.9	13 738 ± 5	811	$t_{2u} + a_{1g} + 63$
17	730.8	13 683 ± 8	866	$t_{1u} + a_{1g}$
18	733.1	13 639 ± 8	910	$2e_g$
19	737.9	13 551 ± 8	998	$e_g + a_{1g}$
20	743.2	13 456 ± 8	1093	$2a_{1g}$
21	749.4	13 345 ± 8	1204	$t_{2u} + e_g + a_{1g}$
22	754.5	13 254 ± 8	1295	$t_{2u} + 2a_{1g}$
23	761.0	13 140 ± 8	1409	$t_{1u} + 2a_{1g}$
24	768.6	13 010 ± 10	1539	$e_g + 2a_{1g}$
25	774.6	12 909 ± 10	1640	$3a_{1g}$
26	780.8	12 808 ± 10	1741	$t_{2u} + e_g + 2a_{1g}$
27	787.5	12 698 ± 10	1851	$t_{1u} + e_g + a_{1g}$

3.2. $^4A_{2g} \rightarrow {}^4T_{2g}$ *TPE spectrum*

Figure 4 is a complete two-photon excitation spectrum of the $^4A_{2g} \rightarrow {}^4T_{1ag}$ transition with the wavevector $\boldsymbol{k}$ and the electric field vector $\hat{\boldsymbol{\eta}}$ parallel to the $\langle 001 \rangle$ and $\langle 100 \rangle$ directions, respectively. Superimposed on the full spectrum in figure 4 is a 35-peak phonon progression, built on the zero-phonon line, with a spacing of 106 cm^{-1}. (Only ten of the 35 peak positions are indicated in figure 4.) The observation of a progression with this number of phonon replicas is unusual because there is no apparent broadening as the number of involved phonons increases. Although a similar progression with 70 phonon replicas and a spacing of 55 cm^{-1} was observed in Mn^{4+}:Cs_2GeF_6 by Chien *et al* [33], such extended progressions are inconsistent with conventional wisdom concerning multi-phonon side bands [34]. When electron–lattice coupling is strong, one expects a broad and symmetrical line shape, generated by overlapping multiple convolutions of a single-phonon side band. The observation of a large number of well resolved phonon replicas in the extended progressions suggests strong coupling either to a single local mode or to lattice modes with a very narrow single-phonon side band.

The 106 cm^{-1} spacing is attributed to a lattice mode involving prominent displacements of the next-nearest-neighbour potassium ions. If it is assumed that the involved ions are behaving as simple harmonic oscillators then frequencies of oscillation should differ by the ratio of the square root of the atomic masses. The 106 cm^{-1} potassium-ion lattice-mode energy then

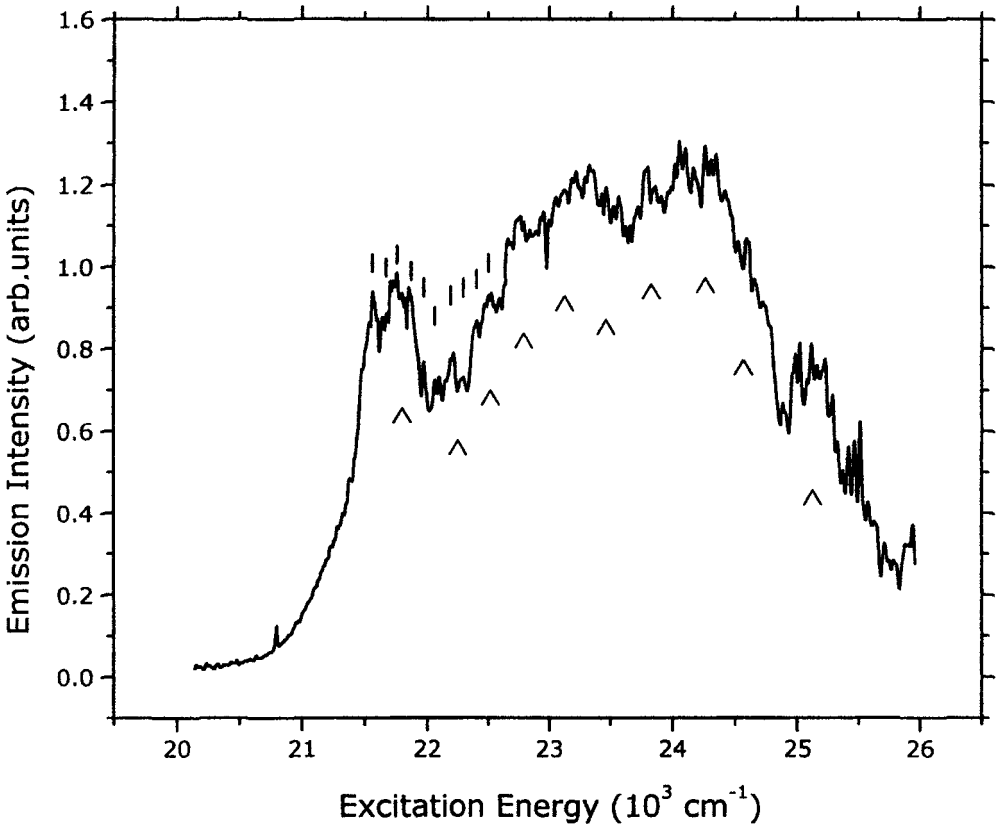

Figure 4. Two-photon excitation spectrum of the $^4A_{2g} \rightarrow {}^4T_{1ag}$ transition in Cr^{3+}:K_2NaScF_6. The laser beam is incident along the ⟨001⟩ direction and polarized along the ⟨100⟩ direction. Positions of sharp lines associated with anomalously extended progressions are indicated, corresponding to phonon energies of 106 cm^{-1} (|) and 310 cm^{-1} (^). Only ten of the phonon replicas in each progression are shown.

compares favourably to the caesium-ion lattice-mode phonon energy of 55 cm^{-1} reported by Chien *et al* [33]. The second progression evident in the $^4A_{2g} \rightarrow {}^4T_{1ag}$ spectrum has a spacing of 310 cm^{-1}. This energy could correspond to the t_{1u} mode shown in low-temperature emission experiments, but odd modes should not appear in TPE spectra. A more likely possibility is a lattice mode involving prominent displacements of the next-nearest-neighbour sodium ions. A more rigorous specification of the relevant normal modes is presented in the following paper (II).

The origin of the broad phonon side band is a split zero-phonon line with its components at 20 634 cm^{-1} and 20 797 cm^{-1}. This region of the spectrum is shown in figure 5, enlarged and at a temperature of 4.2 K. Other experiments have resolved a quartet of zero-phonon lines attributed to spin–orbit coupling [35, 36], with spin–orbit splitting diminished by Ham reduction factors [37] associated with the dynamic Jahn–Teller effect [38]. Since the ratio of peak intensities in the present experiment is inconsistent with this interpretation, the zero-phonon splitting is considered to be the result of the low-temperature phase transition, which presumably suppresses spin–orbit splitting by quenching the orbital angular momentum.

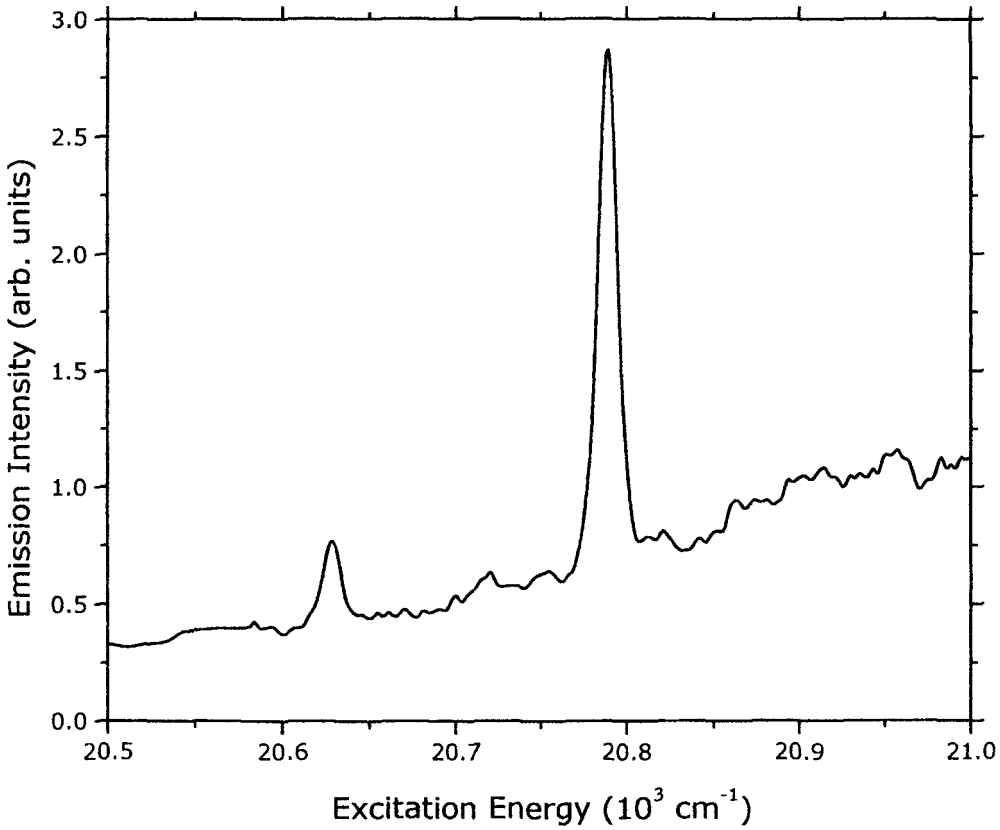

Figure 5. The zero-phonon region of the ${}^4A_{2g} \rightarrow {}^4T_{1ag}$ transition in the Cr^{3+}:K_2NaScF_6 two-photon excitation spectrum. The splitting is 163 cm^{-1}.

Figure 6 is a plot of the normalized integrated emission intensity of the more intense zero-phonon line at 20 797 cm^{-1} as a function of the angle between the polarization $\bar{\eta}$ and the $\langle 100 \rangle$ direction for $\boldsymbol{k}$ parallel to $\langle 001 \rangle$, with data obtained at 4° intervals. The continuous curve in figure 6 is a plot of the expression

$$I/I_0^2 = a + b\sin^2(2\phi) \tag{1}$$

fitted to the data with parameters $a = 3.1$ and $b = 4.2$. The predicted polarization anisotropy for this transition [27] is given by equation (1) with $a/b = 0$; accordingly, the observed polarization anisotropy of the zero-phonon line is anomalous.

Figure 7 is a comparative plot of TPE spectra taken with $\boldsymbol{k}$ parallel to $\langle 001 \rangle$ and with $\hat{\boldsymbol{\eta}}$ parallel to the $\langle 100 \rangle$ and $\langle 110 \rangle$ directions. The spectra are presented with the areas of the zero-phonon lines set equal, i.e. the polarization anisotropy has been removed from the zero-phonon line. Therefore, the deviation of the two different spectra at higher energy is indicative of a wavelength-dependent polarization anisotropy.

The Huang–Rhys factor, S, is a measure of the strength of electron–phonon coupling. It follows from equation (23) of (II) that the Huang–Rhys factor for linear coupling in a configuration-coordinate model is given by

$$S = \ln\left\{\frac{\text{zero-phonon-line area}}{\text{total-sideband area}}\right\} \tag{2}$$

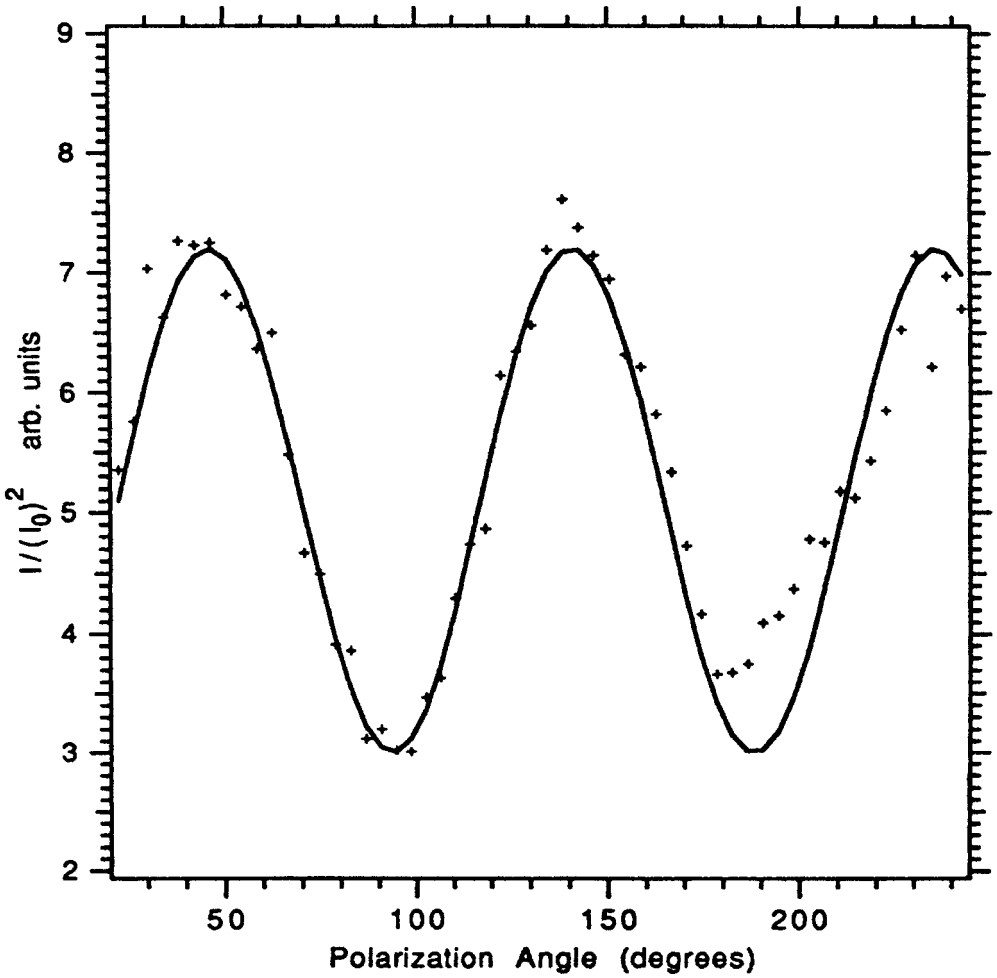

Figure 6. The normalized TPE signal as a function of polarization angle for the 20 797 cm^{-1} zero-phonon line of the $^4A_{2g} \rightarrow {}^4T_{1ag}$ transition in Cr^{3+}:K_2NaScF_6 at 4.2 K. Each data point, indicated by a cross, is the average of 100 shots. The continuous curve is a plot of equation (1) with optimized parameters $a = 3.1$ and $b = 4.2$. The polarization angle ϕ is measured from the $\langle 100 \rangle$ direction with $\boldsymbol{k} \| \langle 001 \rangle$.

as explained in II. This approach yields experimentally determined values of S of 8.4 and 9.4 for the $\langle 100 \rangle$ and $\langle 110 \rangle$ polarized spectra, respectively.

3.3. $^4A_{2g} \rightarrow {}^4T_{2g}$ *TPE spectrum*

Figure 8 is a comparative plot of the $^4A_{2g} \rightarrow {}^4T_{2g}$ spectra taken with $\boldsymbol{k}$ parallel to $\langle 001 \rangle$ and with $\hat{\boldsymbol{\eta}}$ parallel to the $\langle 100 \rangle$ and $\langle 110 \rangle$ directions. It is evident from the equal amplitude spectra that the $^4A_{2g} \rightarrow {}^4T_{2g}$ transition exhibits little polarization anisotropy. It should be stated that this is not an electric-dipole-allowed transition for a two-photon single-beam experiment, according to the work of Bader and Gold [27]. It has been suggested that mixing of the $^4T_{1ag}$ and $^4T_{2g}$ states, via the spin orbit operator, yields a non-zero two-photon transition probability for the $^4A_{2g} \rightarrow {}^4T_{2g}$ band [32]. It is also possible that a low-temperature phase transition,

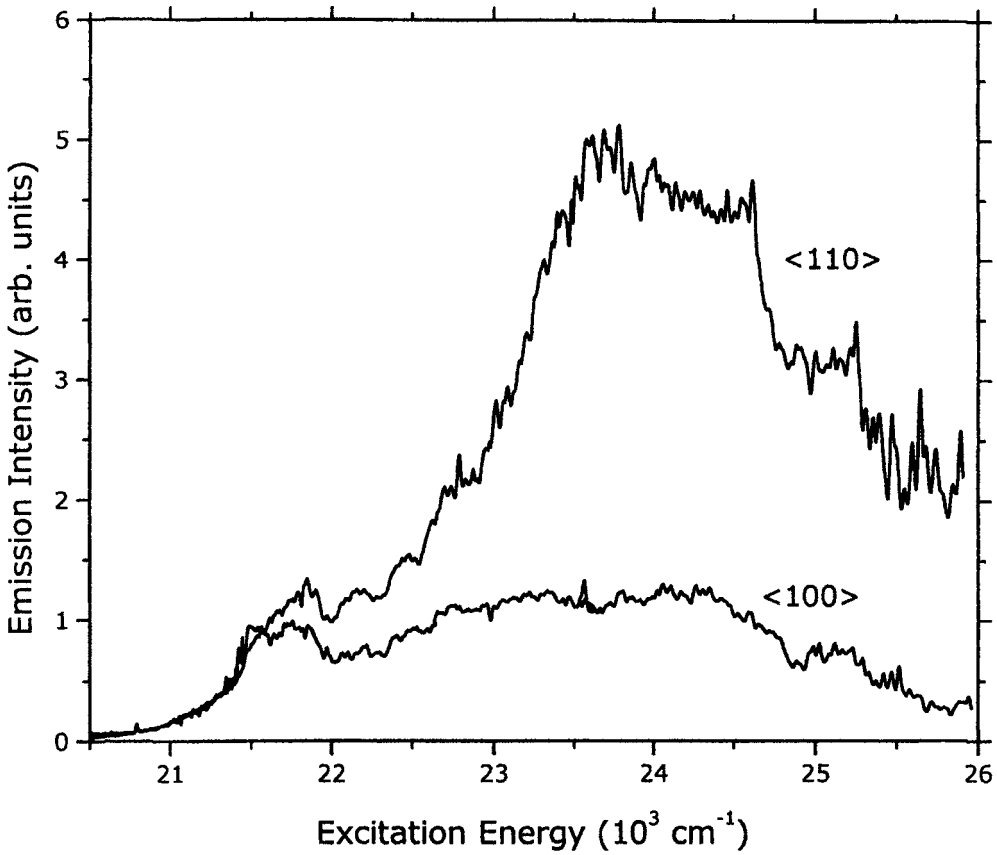

Figure 7. A comparative plot showing the two-photon excitation spectra from $^4A_{2g}$ to $^4T_{1ag}$ in Cr^{3+}:K_2NaScF_6. The laser beam is incident along the ⟨001⟩ direction and each curve is for a different polarization direction. The polarization anisotropy of the zero-phonon line has been removed by setting their areas equal.

known to exist in this compound, could be the method for enabling the $^4A_{2g} \rightarrow {}^4T_{2g}$ transition. However, the absence of a zero-phonon line in the present results makes these two possibilities unlikely.

Emission spectroscopy shows the $^4A_{2g} \rightarrow {}^4T_{2g}$ zero-phonon line is at 14 550 cm^{-1}. The lowest-energy feature of the $^4A_{2g} \rightarrow {}^4T_{2g}$ TPE spectrum shown in figure 8 is a shoulder approximately 450 cm^{-1} above this, attributable to an e-mode false origin. The t_{2g} mode would also enable a two-photon transition but its energy, 228 cm^{-1}, does not match the recorded spectra.

Two features that appear in the two-photon spectra are the Fano-antiresonances associated with the ^2E_g and the $^2T_{1g}$ states. While these have been seen in one-photon experiments [39] where the narrow $^4A_{2g} \rightarrow {}^2E_g$ and $^4A_{2g} \rightarrow {}^2T_{1g}$ spectra overlap the broader $^4A_{2g} \rightarrow {}^4T_{2g}$ spectrum, it is believed that this is the first such identification in a TPE experiment.

There is a progression of broad peaks in the band with a spacing of roughly 500 cm^{-1}. Because no mode of the CrF_6^{3-} octahedron has this energy, the progression is ascribed to an unresolved superposition of progressions of the local e_g and a_{1g} modes with comparable amplitudes. These phonons have ground state vibrational energies of 451 and

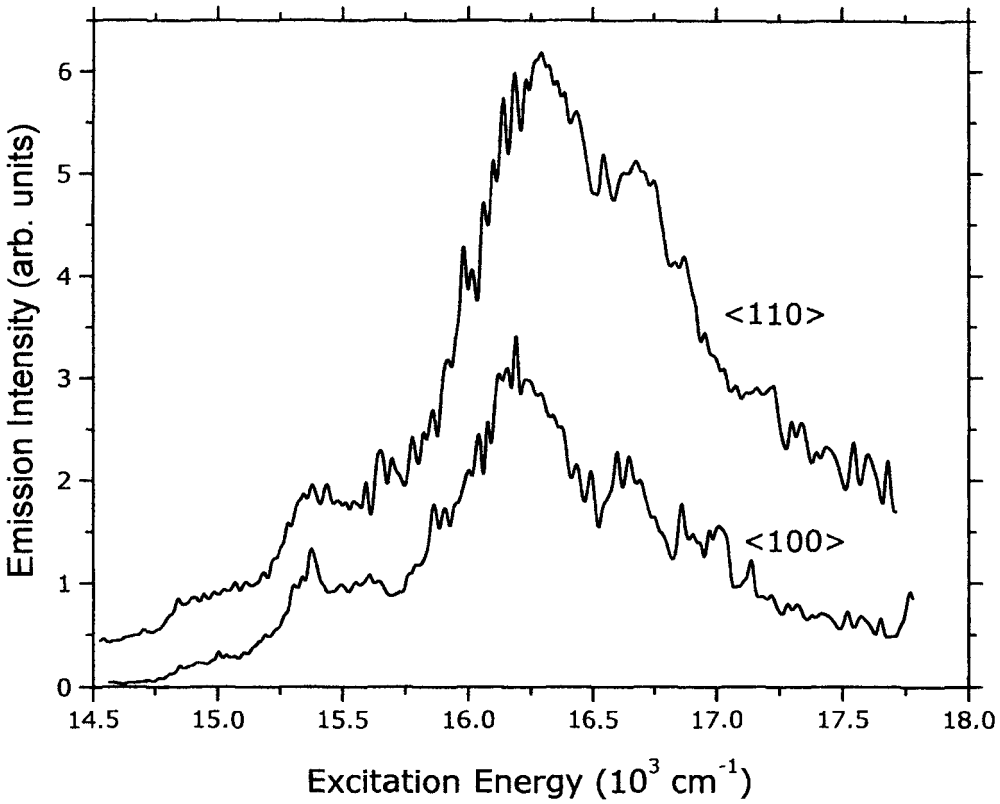

Figure 8. A comparative plot showing the two-photon excitation spectra from $^4A_{2g}$ to $^4T_{2g}$ in Cr^{3+}:K_2NaScF_6. The laser beam is incident along the ⟨001⟩ direction and each curve is for a different polarization direction. A vertical offset of the two curves is introduced for clarity.

541 cm^{-1} respectively. The average energy, 496 cm^{-1}, is comparable to the spacing in figure 8. There is no apparent coupling to the t_{2g} mode.

4. Conclusion

Complete two-photon excitation spectra were recorded for the $^4A_{2g} \rightarrow {}^4T_{1ag}$ and $^4A_{2g} \rightarrow {}^4T_{2g}$ transitions in Cr^{3+}:K_2NaScF_6. Each transition was investigated with $\boldsymbol{k}$ parallel to ⟨001⟩ and with two polarizations, $\hat{\boldsymbol{\eta}}$ parallel to ⟨100⟩ and ⟨110⟩, at a temperature of 10 K.

The $^4A_{2g} \rightarrow {}^4T_{1ag}$ spectra reveal interesting and previously unexplained effects. A phase-transition-induced 163 cm^{-1} splitting was recorded for the zero-phonon line. Superimposed on the side band was a 35-peak phonon progression with a spacing of 106 cm^{-1}, as well as a progression with a spacing of 310 cm^{-1}. The experiments also showed that the side band does not possess the same polarization dependence as the zero-phonon line.

The phonon side band of the two-photon $^4A_{2g} \rightarrow {}^4T_{2g}$ spectrum, lacking a zero-phonon line, originates on an e_g-mode false origin, consistent with the forbidden nature of the purely electronic transition [27]. The generally symmetric excitation spectra possess a single distinct 500 cm^{-1} progression that has been assigned to a nearly equal coupling of the a_{1g} and e_g local modes. The apparent polarization anisotropy and anomalously extended phonon progressions of the $^4A_{2g} \rightarrow {}^4T_{1ag}$ spectra are not present in these spectra. The coupling to a t_{2g} mode is also lacking.

The present paper has described the experimental techniques utilized and the data obtained; the following paper (II) develops a theoretical framework for the analysis of these results.

Acknowledgments

This work was supported by the US Army Research Office under contract No DAAL03-89-K-0059. Elpasolite samples were generously provided by Drs D R Gabbe and B C McCollum.

References

[1] Bartram R H, Wein G R and Hamilton D S 2001 *J. Phys.: Condens. Matter* **13** 2377
[2] Moulton P F 1986 *J. Opt. Soc. Am.* B **3** 125
[3] Moulton P F 1986 *J. Quantum Electron.* **21** 1582
[4] Petricevic V, Gayen S K and Alfano R R 1989 *Opt. Lett.* **14** 613
[5] Walling J C, Peterson O G, Jenssen H P, Morris R C and O'Dell E W 1980 *J. Quantum Electron.* **16** 1302
[6] Payne S A, Chase L L, Newkirk H W, Smith L K and Krupke W F 1988 *J. Quantum Electron.* **24** 2243
[7] Payne S A, Chase L L, Smith L K, Kway W L and Newkirk H W 1989 *J. Appl. Phys.* **66** 1051
[8] Smith L K, Payne S A, Kway W L, Chase L L and Chai B H T 1992 *J. Quantum Electron.* **28** 2612
[9] Berry A J, Denning R G and Morrison I D 1997 *Chem. Phys. Lett.* **266** 195
[10] Tanner P A, Chua M and Reid M F 1995 *J. Alloys Compounds* **225** 20
[11] Chua M, Tanner P A and Reid M F 1994 *J. Lumin.* **58** 356
[12] Deren P J and Strek W 1997 *J. Lumin.* **69** 295
[13] Pawlik T, Spaeth J-M, Otte M and Overhof H 1995 *Radiat. Eff. Defects Solids* **135** 547
[14] McCumber D E 1964 *J. Math. Phys.* **5** 221, 508
[15] McCumber D E 1964 *Phys. Rev.* **134** A299
[16] Andrews L J, Hitelman S M, Kokta M and Gabbe D 1986 *J. Chem. Phys.* **84** 5229
[17] Caird J A, Payne S A, Staver P R, Ramponi A J, Chase L L and Krupke W F 1988 *J. Quantum Electron.* **24** 1077
[18] Sugano S, Tanabe Y and Kamimura H 1970 *Multiplets of Transition-Metal Ions in Crystals* (New York: Academic)
[19] Berg J M, Campochiaro C, Ho D M and McClure D 1992 *OSA Proc. Adv. Solid State Lasers* **13** 290
[20] Sliwczuk U, Bartram R H, Gabbe D R and McCollum B C 1991 *J. Phys. Chem. Solids* **52** 357
Sliwczuk U, Rinzler A G, Kappers L A and Bartram R H 1991 *J. Phys. Chem. Solids* **52** 363
[21] Andrews L J, Lempicki A, McCollum B C, Giunta C J, Bartram R H and Dolan J F 1986 *Phys. Rev.* B **34** 2735
[22] Dolan J F, Rinzler A G, Kappers L A and Bartram R H 1992 *J. Phys. Chem. Solids* **53** 905
[23] Sinkovits R S and Bartram R H 1991 *J. Phys. Chem. Solids* **52** 1137
[24] Woods A M, Sinkovits R S, Charpie J C, Huang W L, Bartram R H and Rossi A R 1993 *J. Phys. Chem. Solids* **54** 543
[25] Bartram R H, Charpie J C, Andrews L J and Lempicki A 1986 *Phys. Rev.* B **34** 2741
[26] Woods A M, Sinkovits R S and Bartram R H 1994 *J. Phys. Chem. Solids* **55** 91
[27] Bader T R and Gold A 1968 *Phys. Rev.* **171** 997
[28] Smith W L 1986 *CRC Handbook of Laser Science and Technology* vol 3, ed M J Weber (Boca Raton, FL: Chemical Rubber Company) part 1
[29] Campochiaro C, McClure D S, Rabinowitz P and Dougal S 1989 *Chem. Phys. Lett.* **157** 78
[30] Barker T J, Denning R G and Thorne J R G 1987 *Inorg. Chem.* **27** 1721
[31] Ferguson J, Guggenheim H J and Wood D L 1971 *J. Chem. Phys.* **54** 504
[32] Greenough P and Paulusz A G 1979 *J. Chem. Phys.* **70** 1967
[33] Chien R L, Berg J M, McClure D S, Rabinowitz P and Perry B N 1986 *J. Chem. Phys.* **84** 4186
[34] Pryce M H L 1966 Interaction of lattice vibrations with electrons at point defects *Phonons* ed R W H Stevenson (New York: Plenum) pp 403–48
[35] Pilla O, Galvanetto E, Montagna M and Viliani G 1988 *Phys. Rev.* B **38** 3477
[36] Manson N B, Hasan Z and Flint C D 1979 *J. Phys. C: Solid State Phys.* **12** 5483
[37] Ham F S 1965 *Phys. Rev.* **138** A1727
[38] Longuet-Higgins H C, Opik U, Pryce M H L and Sack R A 1958 *Proc. R. Soc.* A **244** 1
[39] Sturge M D, Guggenheim H J and Pryce M H L 1970 *Phys. Rev.* B **2** 2459